Comparative Analysis of Novel Iron Oxide Nanoparticles Synthesized by Different Approaches with Evaluation of Their Antibacterial Activities

Wanisa Abdussalam-Mohammed [1,*], Mohammed S. Abraheem [1], Aysha B. Mezoughi [2], Laila Mohamed [2], Mohamed A. A. Alwahsh [1] (ID)

[1] Chemistry Department, Faculty of Science, Sebha University, Sebha, Libya
[2] Chemistry Department, Faculty of Science, University of Tripoli, Tripoli, Libya
* Correspondence: Wan.ahweelat@sehau.edu.ly (W.A.M.);

Abstract: In this study, stable novel iron oxide nanoparticles (IO-NPs) were synthesized via chemical and green methods. In the chemical method, p-aminobenzoic acid (AB), diacetyl monoxime (DIA), and adenosine 5-monophosphate disodium (AD) were used as stabilized ligands, whereas the extract of *Teucrium apollinis* was used in the green synthesis method. The effect of these stabilized ligands on the size, stability, and antibacterial activity of IO-NPs was carried out. The synthesized IO-NPs were characterized using UV-Visible absorption spectroscopy (UV-Vis), dynamic light scattering (DLS), transmission electron microscopy (TEM), and attenuated Fourier transform infrared (ATR-FTIR). IO-NPs offered spherical shapes with small sizes (5 nm, 6 nm, 8 nm, and 34 nm) for IO-NPs functionalized by DIA, AD, AB, and *Teucrium apollinis*, respectively. This study shows a relationship between the type of NPs and Pseudomonas aeruginosa growth. The IO-NP functionalized by plant extract has a higher antibacterial effect than IO-NPs chemically synthesized. Because it has more infinity toward bacteria cells than other NP, it has a high ability to penetrate the membrane of bacterial cells. The use of *Teucrium apollinis* extract could be an eco-friendly way to synthesize IO-NP that offers a novel and potential alternative to chemically synthesized IO-NP.

Keywords: *Teucrium apollinis*; iron oxide nanoparticles; antibacterial activities; Adenosine 5-monophosphate; stability.

1. Introduction

Iron oxide nanoparticles (IO-NPs) with suitable surface chemistry are widely used for several applications such as tissue repair, magnetic resonance imaging contrast enhancement, immunoassay, biological fluid detoxification, drug delivery [1, 2], and cell separation [3]. For example, IO-NPs have many advantages in cancer treatment, cancer diagnosis [4, 5], cancer hyperthermia therapy [6], and demonstrating safety when enjoyed in clinical use for about nine decades [6].

In addition, IO-NPs have demonstrated a promising effect in various biomedical applications based on their sizes, and different synthesis approaches are used [7]. For instance, all biomedical and bioengineering applications need IO-NPs to have sizes smaller than 100 nm. Furthermore, the applications of small iron oxide particles *in vitro* diagnostics have been practiced for approximately 40 years [2]. In the last decade, improved investigations with

various kinds of iron oxides have been carried out in the field of nano-sized magnetic particles (mostly maghemite, γ-Fe_2O_3, or magnetite, Fe_3O_4, single domains of around 5–20 nm in diameter) [2].

The IO-NPs have good biological activity because of their non-toxic role in the biological systems, magnetic behavior [8], and semiconductor properties, which are advantageous for multifunctional biomedical applications [9]. Additionally, it is noted that the IO-NPs have high chemical activity and are simply oxidized in the air (specific magnetite), commonly resulting in loss of magnetism and dispersibility [3]. In the same way, there was a limit to IO-NPs by their inability to reach the site of interest [10].

For this reason, providing appropriate surface coating and developing some effective protection strategies to overcome this limitation and keep the stability of magnetic IO-NPs is very significant.

Several authors have reported that the nature of surface coating ligands on the nanoparticles is not only used to control the overall size of the colloid NPs but also plays a major role in biokinetics and biodegradability of NPs in the body to be suitable for further functionalization [2]. For instance, functionalization of IONPs with suitable ligands is found to introduce further stimuli-responsive behavior, which increases the therapeutic action and effective bio-medical applications [10]. Moreover, organic molecules can give the ensemble functional reactive end-groups, such as aldehyde, carboxyl, hydroxyl, and amino groups. These groups can link to the active bio-substance, like an antibody, DNA, protein, enzyme, etc., for more applications [3].

Furthermore, preparing and functionalizing the IO-NPs with ideal chemicals remains a great challenge for researchers [11]. This study demonstrates well-dispersed water-soluble IO-NPs that are homogeneous IO-NPs with selective surface functionality (NH_2, COOH, OH). These ligands displayed good dispersion in an aqueous solvent and were able to bind to the surfaces of iron oxide nanoparticles efficiently.

Preparing IO-NPs *via* using green chemistry is needed to reduce environmental pollution, as mentioned in the literature [3]. Also, some researchers think that the biological method involving microorganisms and plants is better than physical and chemical methods for the synthesis of nanoparticles [12].

This work uses the petroleum ether extract of *Teucrium apollinis* as a capping agent to stabilize IO-NPs. The genus *Teucrium* (Germander) belongs to Lamiaceae, within the subfamily Ajugoideae. *Teucrium* species are widely used in folk medicine for treating many pathological disorders and are also found to have enormous pharmaceutical benefits. They were very rich in phenolic, flavonoid, and diterpene compounds, with extremely strong biological impacts [13].

Recently, some studies have illustrated that Teucrium contains phenolic compounds, has potent anticancer activity, and offers strong biological activities [13]. For this reason, *Teucrium* extract is used to produce highly stable and water-dispersible IO-NPs for bio-applications. in this work, *Teucrium apollinis* (Lamiaceae) is endemic in Libya, and it is used for the first time as a stabilized ligand for synthesizing iron oxide nanoparticles. The good biocompatibility of these IO-NPs bodes well for their future use in medical applications.

2. Materials and Methods

The synthesis process was started by reacting ferric sulfate $Fe_2(SO_4)_3$ and stabilized ligands in the presence of the reducing agents ($NaBH_4$) in an aqueous solution at room temperature.

2.1. Materials and reagents.

All chemicals and solvents in this work were purchased from Sigma-Aldrich, including ferric sulfate $Fe_2(SO_4)_3$, sodium borohydride (98.0%) ($NaBH_4$), p-aminobenzoic acid (AB), Adenosine 5-monophosphate disodium salt (AD), and Diacetyl monoxime (DIA).

2.2. Characterisation techniques.

Several analytical techniques were used to characterize IO-NPs, including UV-Vis, TEM, DLS, and ATR-FTIR. The stability of the IO-NP was monitored by using the UV-Visible technique.

2.2.1. Ultraviolet-visible absorption spectroscopy (UV-Vis).

UV-visible spectra were obtained on an Evolution 300 spectrophotometer with a double beam principal system with data recording via using the Vision software version on Windows XP/2000. Three measurements were taken from each sample for good accuracy. The surface plasmon resonance (SPR) band of IO-NP samples was recorded in the 200-800 nm range. All IO-NPs samples in this work showed a characteristic SPR band between 259 nm and 383 nm.

2.2.2. Dynamic Light Scattering (DLS).

The Dynamic Light Scattering (DLS) technique (Zetasizer Nano ZS (Malvern Instruments Ltd) was used to measure the size and size distribution of NPs. The sample was placed into a quartz cuvette. Three measurements were taken from each sample after calibration of the equipment. The data was collated into a size distribution.

2.2.3. Transmission Electron Microscopy (TEM).

TEM is the best technique used to determine the morphology, size, and shape of NPs. A JEOL2100 field emission gun transmission electron microscope (FEG TEM) set at 100 KV was used for the analysis of the particles and to obtain the TEM micrographs. The size distribution was obtained via counting and measuring about 150 IO-NPs. The deposition method was applied to prepare the samples for TEM analysis. The drop of diluted IO-NPs was placed and suspended on a holey carbon-coated copper grid.

2.2.4. Attenuated total reflection-Fourier Transform Infrared Spectroscopy (ATR-FTIR).

ATR-FTIR spectroscopy (Bruker Tensor 27, Germany) was used to examine the samples directly in the solid or liquid state without further preparation. ATR-FTIR spectra of the IO-NPs and ligands were recorded in the 400 to 4000 cm^{-1}, and a background spectrum was recorded before each analysis. Spectra were analyzed using Origin software (Version 7.5) equipped with a Peak-Fitting Module (PFM).

2.3. Synthesis of iron oxide nanoparticles by chemical ligands.

Several recent preparation strategies have been developed to adjust the IO-NPs properties [3]. Controlling the properties of iron oxide NPs is necessary for the desired application. Different methods were used to prepare IO-NPs, such as laser ablation, hydrothermal method, chemical co-precipitation, etc. However, solution combustion synthesis, among all these methods, is a promising alternative for synthesizing a large number of metal oxide nanoparticles with multiple advantages, such as short preparation time, simple procedures, cheap starting materials, high efficacy, and low-cost apparatuses [14].

The biocompatible colloidal suspensions of iron oxide nanoparticles coated with four different ligands were prepared in this work and followed the literature method with a slightly modified [15].

2.3.1. Synthesis of IO-NPs functionalized by p-Aminobenzoic acid, adenosine 5-monophosphate disodium salt, and diacetyl monoxime.

With vigorous stirring, (0.0041g, 0.029 mol), (0.0117 g, 0.033 mol), and (0.0030 g, 0.029 mol) from *p*-aminobenzoic acid (AB), Adenosine 5-monophosphate disodium salt (AD), and Diacetyl monoxime (DIA) respectively were dissolved in 30 ml of distilled water. Then these mixtures of stabilized ligands were added to ferric sulfate solutions (ferric sulfate $Fe_2(SO_4)_3$ (0.0039 g, 0.009 mol) was dissolved in 20 mL of distilled water) and left to stir for 2 hours at rt. The colors of solutions were changed when a reducing agent (2 mL of freshly prepared $NaBH_4$) (0.0013g in 10 mL of distilled water) was added to later mixture solutions from colorless to light brown, dark brown, and reddish-brown, respectively, indicated to produce iron oxide nanoparticles. The mixtures were left to stir for an additional 2 hours to ensure that the reactions were completed. For the consequent characterizations, the samples were washed by centrifuging and re-dispersing three times with (distilled H_2O/EtOH) (2:1), to remove the residual chemicals. The preparation procedure was done three times to confirm IO-NPs were synthesized, and the results were quite the same. The samples were kept under normal laboratory conditions.

2.3.2. Synthesis of IO-NP using extraction of *Teucrium apollinis*.

The aerial parts of *Teucrium apollinis* were collected from the Slop Mountains of Ras El-Hilal, Cyrenaica region, Libya, during the flowering stage in April 2021. The plant was identified by Dr. Abdossalam Elmogassapi, lecturer in the Department of Botany, the College of Science, University of Benghazi, Libya.

2.3.2.1. *Teucrium apollinis* extraction procedure.

In brief, the aerial part of the plant was cleaned and dried in the shade. After that, the plant was ground by an automatic mill to get the dry plant powder. This powder was extracted with petroleum ether (40-60 °C) using a continuous extraction device (Soxhlet) until exhaustion. Then the solvent was evaporated using a rotary evaporator at 40 °C to obtain the petroleum ether plant extract used in this study.

$Fe_2(SO_4)_3$ (0.0039 g, 0.009 mol) was dissolved in 30 ml of distilled water in a conical flask. 0.0090 g of extract plant as a stabilized ligand was added to the last mixture and left to stir for 2 hours. At this time, a yellow-green color appeared and changed to a dark green/brown once 5 mL of the freshly prepared $NaBH_4$ (0.0013 in 25 mL of distilled water) was added step

by step to the last mixture; the vigorous stirring was continued for an extra 2 hours as described in Figure 1. The UV-Vis was confirmed as IO-NP produced.

Figure 1. Preparation procedure of iron nanoparticles using an extract of *Teucrium apollinis* added to the ferric sulfate solution with NaBH4 as a reducing agent.

2.4. pH measurement.

It is well mentioned that the pH value is one of the important factors in synthesizing metal nanoparticles, where different sizes of NPs are produced based on the control of the pH [16]. According to previous literature, it was found that the addition of acid or base to the nanoparticles changes the sizes of IO-NPs. For instance, iron oxide nanoparticles (35-45 nm) are produced at pH 10 with ferromagnetic behavior. While in an acidic medium, the larger maghemite IO-NPs (50-60 nm) were obtained based on TEM and SEM results [17].

The investigation of the influence of pH changes on synthesized IO-NPs by varying the addition of hydroxyl ions (OH^-) and hydrogen ions (H^+) was done in this study. Based on previous studies, different pH levels influenced the properties of NPs, such as the degree of aggregation/agglomeration, stabilization, and antibacterial activity [18, 19]. Set volumes of 1M HCl and 1M NaOH (5-30 µL) were added step by step to water-soluble IO-NPs. The pH-adjusted IO-NP dispersions were then sonicated in a water bath for 10 min to guarantee uniformity across the solution. After being set at room temperature for another 10 min, the pH value was rechecked to ensure the targeted pH values. When there were no pH changes in the IO-NP solution, the SPR of the NP dispersion was studied with UV-Vis. At this point, three absorbance evaluations are taken for each value in the pH range.

In this work, the pH of functionalized IO-NPs dispersed in water has changed *via* adding different amounts of 0.1M HCl and NaOH (5-30 µL) with vigorous stirring, the UV-Vis analyses were carried out to determine whether aggregations occur or not.

2.5. Biological study.

The bioactivity of IO-NPs against Pseudomonas aeruginosa bacteria strains has been studied in this work, where the maximum sensitivity of our nanoparticles is confirmed by optical density measurements (OD). The method was done according to an established procedure [20]. The samples were incubated for 6 hours at 37°C. The samples' optical density at 600 nm (OD600) was evaluated at various time intervals of incubation from 0, 1, 2, 3, 4, 5 6 hours by using a UV-Vis spectrophotometer (Jenway model 6305, UK). The antibiotic (imipenem10µg) is used to be compared with IO-NPs samples, and inhibition of bacterial

growth is valued from OD_{600} after 6 hours of incubation. The GRAPHPAD PRISM V5.00 software (the ANOVA test ($p < 0.05$) is used to analyze the obtained data.

3. Results and Discussion

In this study, aqueous $Fe_2(SO_4)_3$ is reduced by freshly aqueous $NaBH_4$ in the presence of various coating agents. The formation of IO-NPs was indicated by the appearance of brown color, which was usually completed in 4 hours. Our study emphasizes that the effect of stabilized ligands resulted in different stabilities and sizes of IO-NPs, where sizes were obtained from 6 nm to 51 nm.

3.1. UV-visible Spectroscopic Investigation.

UV-Vis was used before other techniques to confirm IO-NPs production and their stability; the water-soluble IO-NPs were monitored weekly for every single sample alone for more than 12 weeks. The UV-Vis spectra of IO-NPs were analyzed at a wavelength of 200–800 nm. The absorption at 259–383 nm wavelength confirmed that IO-NPs are produced.

3.1.1. Study of the iron oxide nanoparticle's stability.

The stability of freshly synthesized samples of water-dispersed IO-NPs of the four capping agents was monitored for the duration of around 12 weeks of storage at a normal laboratory condition. The UV-Vis measurements were taken on different days, and the results are presented in Figures 2 and 3. The samples were analyzed at the initial time (freshly prepared), one week, and then from 2 to 12 weeks after the synthesis. The maximum absorbance wavelength shift is observed during the storage, which decreases the stability of IO-NPs with time, which confirms previous studies [21]. Also, observation showed that the colors of dispersed IO-NPs changed slightly to be darker after more than 12 weeks compared with freshly synthesized IO-NPs, which confirms that the iron oxide NPs core size and colloidal stability are changing over time.

According to El-Sayed *et al*., the position of the maximum absorbance measured with UV-Vis depends on many factors, such as the shape, the surrounding media, the dielectric constant, and the size of the nanoparticles [22]. Herein, all UV-Vis showed the formation of IO-NPs, and all peaks were centered at 259–383 nm. The intensities of peaks were different with functionalized ligands used, as shown in Figures 2 and 3.

The choice of ligands is extremely important for nanoparticle function and colloidal stability. The selection of some kinds of ligands utilized in nanoparticle synthesis is responsible for their final size and shape [23]. In addition, there was a difference in the rate of IO-NPs formation using different coating ligands if compared with each other. Formation of IO-NPs using *Teucrium apollinis* extract took a shorter time (2 h) than other chemical ligands used in this work, maybe due to its chemical structure, which has more affinity toward the IO-NP surface.

It is well-mentioned that the functional groups of stabilized ligands contribute significantly to controlling the stabilities and sizes of NPs with the previous data published by other studies [24]. Likewise, it is confirmed that ligands used to functionalize nanoparticles containing carboxyl groups are found to provide a stabilization effect. For instance, carboxyl and hydroxyl groups in coating ligands have a strong binding affinity toward IO-NPs [22],

compared with thiol groups, which are known to have a high affinity toward gold NPs surfaces [25].
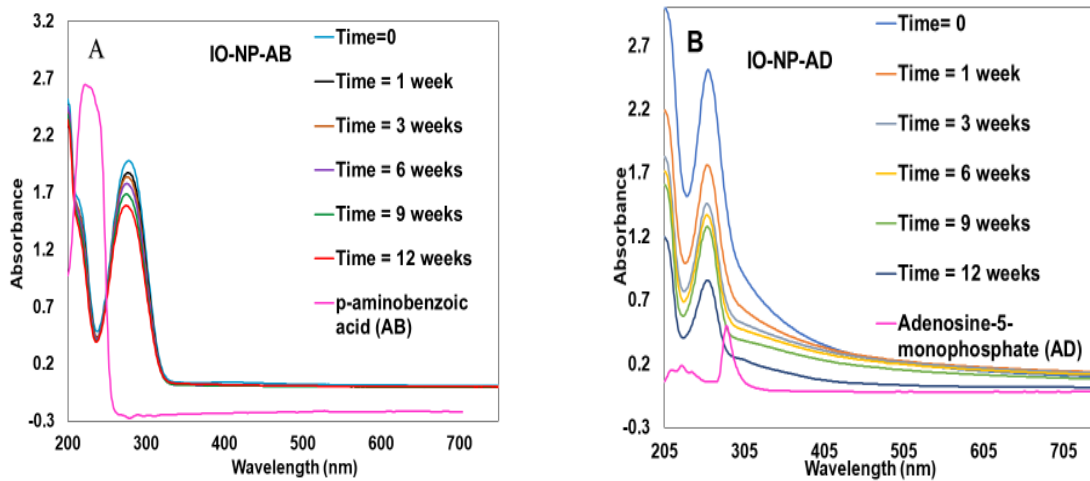

Figure 2. UV-Vis spectra show the stability of IO-NP over 12 weeks. (**A**) *p*-aminobenzoic acid stabilized IO-NPs, (**B**) IO-NP stabilized by Adenosine 5-monophosphate disodium. It is illustrated that the absorption peaks were at a wavelength of 272 nm and 260 nm, respectively, at the initial time (time =0). The UV-Vis was measured for the ligands alone (see Figure 2 (**A**, **B**) purple lines), which have a different wavelength from IO-NPs functionalized by the same ligand.
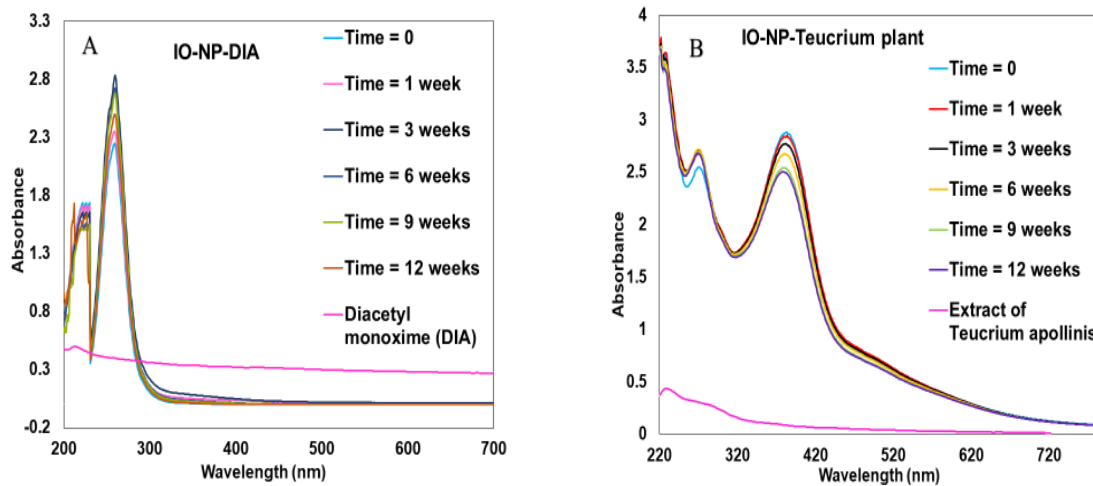

Figure 3. Surface plasmon resonance was measured with UV-Vis at a wavelength of 259 nm and 383 nm core size. Diacetyl monoxime (DIA)(**A**) and extract of Teucrium (**B**) capped IO-NPs is measured in a period of 12 weeks, respectively. The UV-Vis for only these capping ligands (purple lines) was measured to confirm their different absorbance with NP produced.

Herein, the attachment of AB, DIA, AD, and *Teucrium apollinis* extraction on the surface of IO-NPs was predicted through its carboxyl and hydroxyl functional groups. The wavelength peaks indicate the formation of different sizes and shapes of IO-NPs. Figure 2 (A) and (B) illustrate the wavelength band of IO NPs for large and small-sized spheres, respectively. Initially, after AB-IO-NP was produced, we observed a peak at 272 nm (Figure 2, curve A), which shifted to 280 nm after 12 weeks from the initial time of preparation. This peak became a little broader, but there is no evidence that any aggregation may occur. The shifting of the λ_{max} value towards higher wavelengths with an increase in time indicates the formation of larger particles or the agglomeration of smaller particles based on other studies [26].

However, low stability was noted when AD was used to stabilize IO-NP after nearly 12 weeks, where the wavelength was at 260 nm and changed to 270 nm, indicating a large size and reducing its stability after 12 weeks. The reason may be due to the presence of an amino group, which has a little bit less affinity than other functional groups [27] (see Figure 2, curve B). In addition, IO-NP stabilized by AD, which contains amino and hydroxyl groups in its structure, led to increased stability of IO-NP. The presence of both hydroxyl and amine residues in the stabilized ligands enhances the specific interaction of these ligands with the surface of metal oxide NPs. It provides high stability of suspension NP, as illustrated in the previous study, which confirmed our result in this study [28].

In addition, when diacetyl monoxime (DIA) was used as a coating agent of IO-NPs (see Figure 3, curve A), a significant difference was noted, as well as long-term stability. The size was smaller than other IO-NPs in this study. It has stayed stable for more than 12 weeks with similar sizes. This is because DIA has a high affinity for the IO-NP surface. This ligand affords the free surface carbonyl (C=O) group, which, as mentioned by researchers, is necessary for further covalent bonding with the targeted molecules [29].

It is hard to produce IONP via green synthesis due to the presence of polyphenols and antioxidants, which shield the NPs from aggregation and oxidation [30]. The plant extraction used in this work has not shown any evidence for extra stability of IO-NP despite condition changes. The Teucrium extract-IO-NPs (Figure.3, curve B) showed the biggest size in this work due to its chemical composition, which contains phenols and many alkaloids [13]. Also, comparing the tendency to aggregation between IO-NP stabilized by chemical ligands and plant extract shows that the polyphenols act as covering agents; this agrees with the previous results [31].

The comparison between these ligands and their corresponding IO-NPs is shown in Figures 2 and 3; this detailed comparative analysis has thus confirmed the successful binding of these ligands on the IO-NPs surface.

3.2. Dynamic Light Scattering (DLS) analysis.

Dynamic light scattering (DLS) is also known as one of the most widely applied measuring techniques used in determining the size of nanoparticles in liquid media [32]. DLS measurements of the above ligands capped IO-NPs were performed after 30 minutes of exposing IO-NPs to different dilutions. As required for medical purposes, such as hyperthermia treatment or magnetic resonance imaging, the particle diameter should be less than 100 nm with high stability [33] and without forming large aggregates [34].

It has long been a scientific and technological challenge to produce modified size and shape magnetic nanoparticles. For example, physical methods such as gas-phase deposition and electron beam lithography are elaborate procedures that suffer from the inability to control the size of nanoparticles in the nanometer size range, as demonstrated in the literature [2]. In this paper, highly stable and water-dispersible IO-NPs are produced in the same conditions with narrow size distributions, which were in the range of (4.8-7.5 nm, 6.3-8.72 nm, 10.2-14.2 nm, and 47-56 nm) depending on the stabilized ligand used. Where IO-NP sizes were ordered as DIA-IO-NP > AD-IO-NP > p-aminobenzoic acid-IO-NP > *teucrium apollinis* extract-IO-NP (see Figure.4 ⁽⁽A to C⁾⁾). The smallest size was produced when DIA was used as a functionalized ligand. This ligand-bearing OH group is in resonance with C=N, and it is known that using multidentate anchoring groups on ligands was found to increase the binding strength and, thus, the stability of colloidal nanoparticles [35]. The results of UV-Vis of all IO-NPs and

DLS have confirmed each other in this study and indicate the monodispersed nature of the formed IO-NPs. It is well mentioned that DLS is considered to be one of the most commonly used techniques used to measure the size characterization of NPs. However, hydrodynamic size measurements obtained through DLS were conducted not only on the metallic core but also with all substances that covered the surface of NPs, as previous research has shown [36].

It can be concluded that the size of the IO-NPs increased when AB ligand was used due to the present carboxyl group in the aromatic compound that results in big size compared with aliphatic carboxylic acid, which produced smaller sizes of NPs, and this confirmed that ligands are attributed the effect of modifying the growth phase as a similar observation was made by earlier reports [37].

Another study illustrated that surface treatment with aromatic ligands containing COOH groups (such as 4-mercaptobenzoic acid (MBA), and benzoic acid) led to better iron nanoparticle dispersion compared with aliphatic acid-like propionic acid, probably as a result of the higher polarity of aromatic acidic ligands compared to their aliphatic counterparts [36].
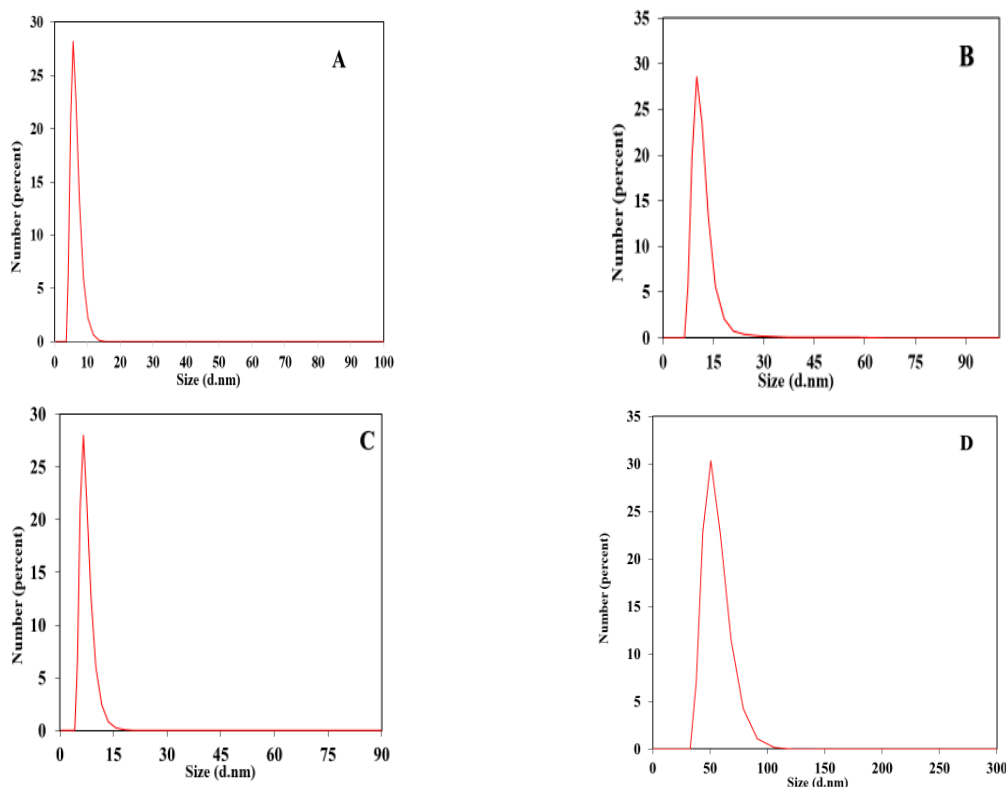

Figure 4. The hydrodynamic size of the synthesized IO-NPs was investigated by DLS analysis in a colloidal solution. Where the DLS diagram of IO-NPs dispersed in water coated by DIA, AB, AD, and *teucrium apollinis* extract plant (A, B, C, and D) respectively. The samples were placed into a quartz-cuvette, and three measurements were taken from each sample after calibration of the equipment. It shows that there is no sign of IO-NPs aggregations in these high ionic strength solutions. DLS images represent the sizes of IO-NPs where A= DIA-IO-NP 6± 1.9 nm, B = p-Aminobenzoic acid-IO-NP 12 ± 2.2, C =AD-IO-NP 8± 0.7 nm, D = *Teucrium apollinis* extract-IO-NP 51 ± 3.8 nm. From the results, it can be concluded that the size of the IO-NPs changed with the change in the capping ligands.

3.3. TEM Results.

IO-NPs were successfully functionalized by DIA, AB, AD, and *Teucrium apollinis*. Based on TEM results, the IO-NPs are monodispersed and have a spherical shape with a narrow size distribution (see Figure 5 (A, B, C, and D)). The mean particle diameters were obtained by calculating the averages and standard deviations. The average particle sizes for IO-NPs

synthesized by DIA, AB, AD, and *Teucrium apollinis* were 5 ±1.2 nm, 8 ± 0.9 nm, 6 ± 0.9, and 34±3 nm, respectively. At least 150 particles were analyzed per sample, and numerous images were captured. The iron oxide nanoparticles were stable, and there was no evidence of the agglomeration of particles. The results of TEM confirm the DLS results. As a consequence, this capping offered high stability for IO-NPs.
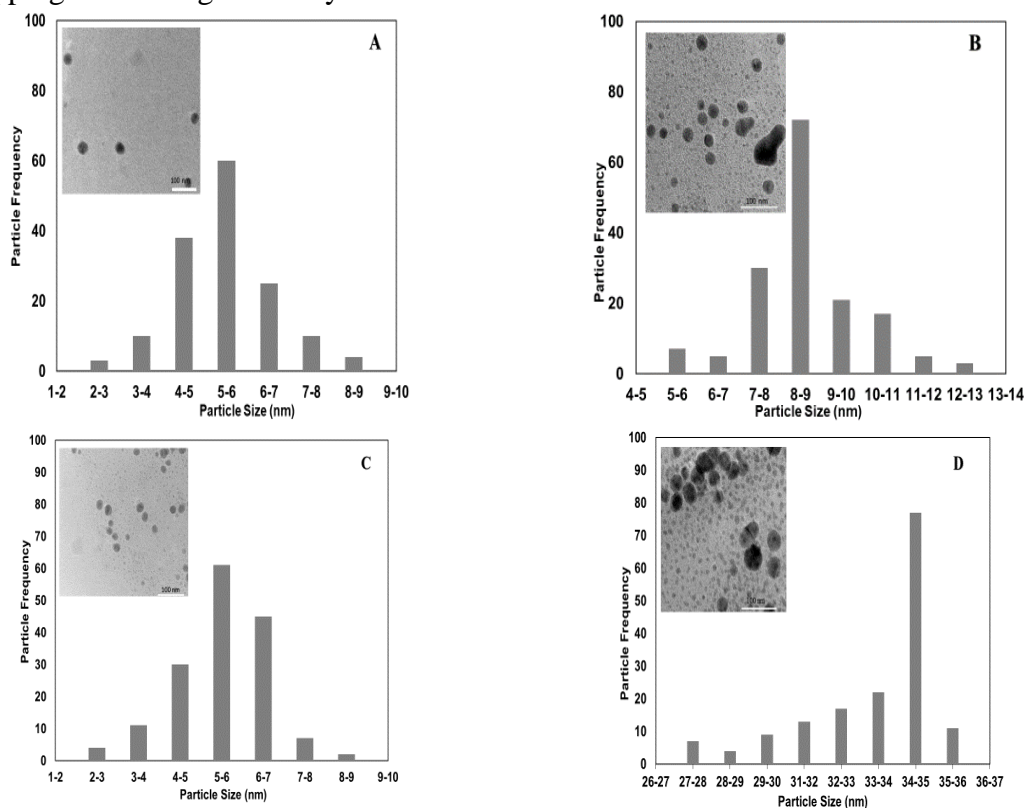

Figure 5. Demonstrative TEM micrographs of IO-NPs synthesized by DIA (**A**), AB (**B**), AD (**C**), and *Teucrium apollinis* (**D**) as protecting ligands, respectively. IO-NPs are formed in a spherical shape with a 5–34 nm size.

3.4. Attenuated total reflection Fourier Transform Infrared Spectroscopy (ATR-FTIR).

Spectroscopy analysis of IO-NPs was performed to detect intermolecular chemical interactions and structural changes of NPs, as mentioned in the literature [35]. Figure 6 (A to D) shows the ATR-FTIR spectra of IO-NPs functionalized by DIA, AB, AD, and *Teucrium apollinis* extract and their comparison with these ligands, respectively. The first curve (black line) and the second curve (red line) are the IR bands of pure stabilized ligands and IO-NPs stabilized by the same ligands.

The band at 1735 cm^{-1} could be attributed to the C=O stretching of DIA, which shifted to a lower wavenumber at 1660 cm^{-1} in IO-NP functionalized by this ligand, which means reduced to a single band in the case of IO-NPs. This decrease is indicated by a strong interaction between the carbonyl group on the DIA with the surface of IO-NP [38].

The band at 1404 cm^{-1} indicated a methyl group's C–H bending mode in DIA, and the same band was also observed in the DIA-IO-NP [39].

In addition, the (C=O) peak for *p*-aminobenzoic acid appeared at 1658 cm^{-1}, which disappeared in *p*-aminobenzoic acid-functionalized IO-NP. Previous research has shown that this contributes to the carboxyl group's functionalization of IO-NPs [40].

Furthermore, the peak at 1589 cm^{-1} in this ligand indicated (C-O), which shifted toward 1625 cm^{-1} in IO-NP. The peaks at 3464 cm^{-1} and 3364 cm^{-1} in *p*-aminobenzoic acid are due to

the (NH_2) group. The (C=O) peak for *Teucrium apollinis* appeared at 1705cm^{-1}, which shifted to 1650 cm^{-1} for IO-NP functionalized by this ligand.

As mentioned earlier, IR was used to analyze the presence of various functional groups on the surface of the iron oxide nanoparticles before and after coating. The (C-O) peak for AD (see Figure 6 curve C) appeared at 1658 cm^{-1}, which shifted to 1635 cm^{-1} for IO-NP functionalized by this ligand. The OH and NH_2 groups range from 3109 cm^{-1} to 3394 cm^{-1} in the case of the AD ligand, which also shifted after functionalized IO-NP to the range from 3200 cm^{-1} to 3425 cm^{-1}. The absorbance at 1357 cm^{-1} in IO-NP was referred to (C-O), while this peak is shifted toward 1381 cm^{-1} in AD, confirming the interaction of AD on the surface of IO-NP. Furthermore, the band observed at 1100 cm^{-1} in IO-NPs was shifted from 1033 cm^{-1} AD ligand, corresponding to P-O asymmetric stretching [41]. In addition, IR results showed broadband located at 3217 cm^{-1} in DIA-IO-NP (red line), which is shifted to 3100 cm^{-1} in the case of the only DIA ligand (black line), corresponding to the stretching vibration of the hydroxyl group (–OH) (see Figure 6A) [39].

Furthermore, the peak at 2917 cm^{-1} in the *Teucrium apollinis* extract curve is due to an aromatic ring. This peak has been shifted to 3116 cm^{-1} in the case of an IO-NP sample functionalized by *Teucrium apollinis*, indicating their interaction. The broad peak in the range of 3200–3500 cm^{-1} in both the IO-NPs curve spectra indicates the presence of –OH groups. The two bands at 2850 cm^{-1} and 2920 cm^{-1} are related to vibrations of symmetric and asymmetric methylene and methyl groups, as shown in Figure 6 (curve D).

These dramatic differences in infrared absorption bands between IO-NPs and the stabilized ligands indicated a strong interaction between the iron oxide nanoparticles and these ligands without any fundamental change in their chemical structures. The presence of these functional groups (hydroxyl, amine, and carboxyl) on the surface of functionalized IO-NPs was confirmed using ATR-FTIR. This means that the synthesis of IO-NPs by these biomolecules was successfully done in this study.
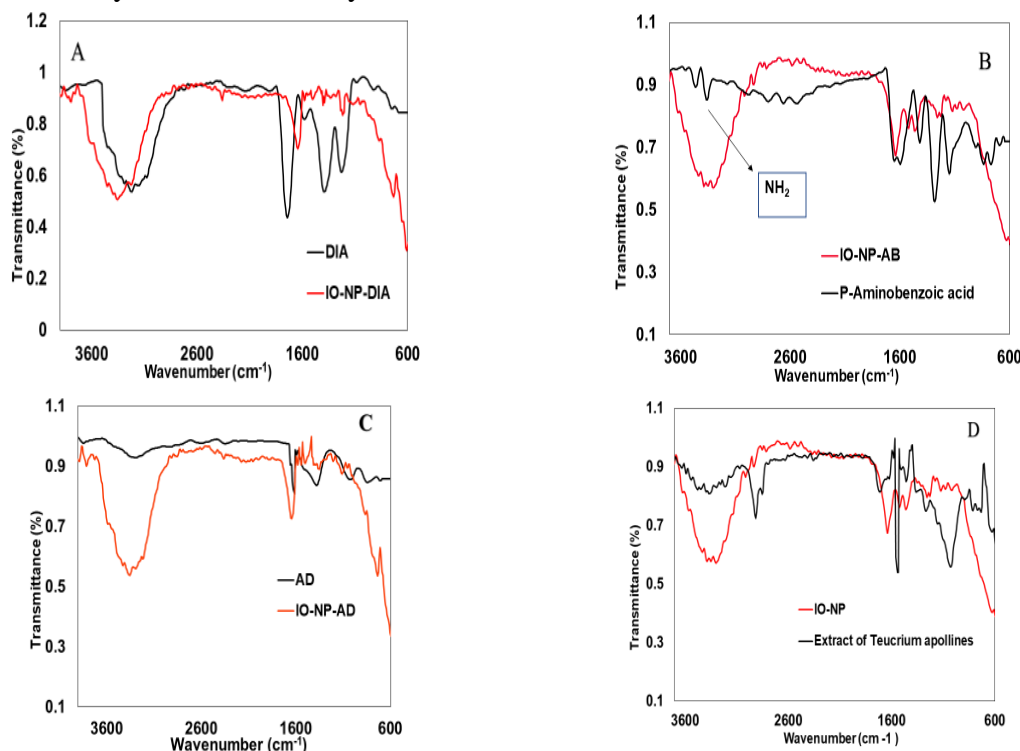

Figure 6. ATR-FTIR spectra of IO-NPs functionalized by Diacetyl monoxime (DIA (**A**)), p-aminobenzoic acid (AB (**B**)), Adenosine 5-monophosphate disodium (AD (**C**)), and *Teucrium apollinis* extract (**D**) stabilized the IO-NPs. The comparison between these ligands (black line) and nanoparticles produced was made (red line).

3.5. pH Results.

The IO-NPs in this study offered high stability in aqueous suspension. Where the appropriate stabilized ligands are used to synthesize highly uniform and monodisperse IO-NPs, they achieve sufficient repulsive interactions to prevent any agglomeration. However, small aggregate NPs are formed with either low or high pH values. According to Wittmann *et al.*, the aggregation behavior of IO-NP is influenced by pH changes, which confirms our results [33].

According to the previous study, IO-NPs were not easy to suspend in water because they were completely agglomerated [18]. In contrast, IO-NPs functionalized by our ligands showed high stability with water dispersed. In addition, the effect of pH on the formed nanomaterials was investigated in detail. For example, the IO-NPs size was smaller at lower pH than at neutral pH because agglomeration increased when the pH changed from 2.0 to 7.0 based on the literature results [18]. In this work, we have investigated the influence of pH on the stabilities of IO-NPs functionalized by different ligands bearing different functional groups in their structures.

In addition, ligands with carboxyl and hydroxyl groups (such as citrate) adsorb onto the surface of gold nanoparticles via their carboxyl groups. Changes in pH significantly affect their affinity toward the gold NP surface. At neutral pH, only the central carboxylate group is adsorbed on the surface of NPs [22]. In contrast, both the carboxyl and hydroxyl groups are adsorbed at a high pH (pH $\geq$ 11) [22]. Furthermore, the surface iron atoms of the iron oxide NPs act as Lew's acids and can easily coordinate with molecules that donate lone pairs of electrons [22], such as NH_2, OH, etc., which encouraged us to choose these ligands in this work. The stability of IO-NPs was monitored with pH changes. For example, Figure 7 shows the measurements of pH of IO-NP-p-aminobenzoic acid in alkaline and acidic mediums (A and B), respectively. At the initial time, the SPR was 272 nm at pH 4 - 4.5. This wavelength was changed to 280 nm after HCl was added (30 µL), which indicates that it was changed to be bigger than freshly prepared IO-NP. The same change was noted when a high amount of NaOH (30 µL) was added, and the pH became 10.7. The SPR was 284 nm, which confirmed the effect of pH on the size of nanoparticles and their stability, whereas IO-NP-AB at pH ranging from 5,1 to 7.4 remained almost stable.

Similar results were noted when other ligands were used to functionalize IO-NPs. For instance, IO-NPs-AD offered a small size with high stability at pH 5.1-pH 9, and no evidence was shown for any aggregation through this range. The size was gradually increased at high pH (pH > 9) and at low pH (pH < 2), and the precipitation was steadily observed at pH values close to pH 1.8 and pH 13.

The wavelength of IO-NPs-AD changed from 260 nm at pH 5.1 to 300 nm, when pH decreased to 1.4, indicating that agglomeration and big size occurred (see Figure.7, curve D). Also, the decrease in stability of NPs was noted in high basic conditions, where agglomerated IO-NP was shown at pH 13 (see Figure 7, curve C). These results concluded that the size of the iron oxide nanoparticles was impacted and changed by the change in pH levels. Thus, natural pH values result in a smaller size of IO-NPs, which aggregate as pH increases or decreases. That may be a significant goal for different applications, as mentioned in the literature [18].
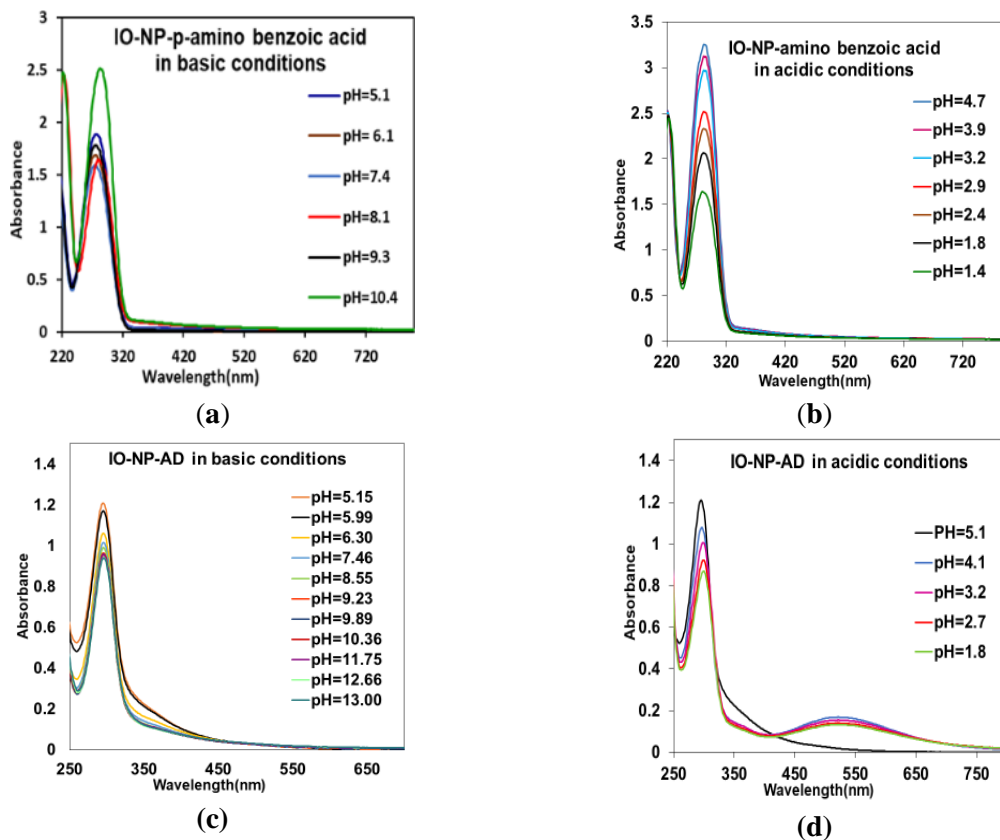
Figure 7. UV-Vis data collected at the pH range formed by adding HCl (0.1M) and NaOH (0.1M) to the AB-IO-NPs and AD solutions, (a) (c) at pH > 7.5, and pH < 7.5 (b) (d) respectively. It can be observed that the shape and height of the surface plasmon bands change as well as the pH changes.

The reason for appearing in this aggregation is because the carboxyl groups are partially protonated under these highly acidic conditions, and they undergo deprotonation reactions in highly basic media [15].

3.7. Antibacterial activities of iron oxide nanoparticles.

Most hospital and community-born infections were caused by pseudomonas aeruginosa, leading to serious therapeutic challenges in treating these infections [42]. This kind of bacteria was chosen as a model in this study as a result of its prevalence and importance in human diseases [43]. It is necessary to find suitable therapy against resistant strains of pseudomonas aeruginosa.

The main advantage of IO-NPs is their magnetic properties that allow direct delivery of the substance to the region of the pathogen without affecting the whole organism, which encourages an increasing interest in the development of antimicrobial IO-NPs [44]. As known, NPs have a high surface-to-volume ratio that increases reactivity and potential biochemical activities. In comparison, the interaction mechanism between NPs and biological systems is still largely unknown [45].

Surface modification and additional functionalization for IO-NPs are required to improve their biocompatibility, which is found to be beneficial in decreasing the unexpected damage to healthy tissues [46]. According to an established study, the plant functionalized IONP has many advantages compared to other chemicals, and physical and biological modes of NP synthesis [47].

Currently, many studies have been published showing that IO-NPs have antimicrobial effects against Gram-positive and Gram-negative bacteria. Others demonstrated that IO-NPs

have relatively weak antimicrobial activity [48] against many strains and poor biocompatibility with eukaryotic cells [49]. The antibacterial activity of the synthesized iron oxide nanoparticles against multi-drug-resistant *pseudomonas aeruginosa* is shown in Figure 8. The mechanisms of NPs inhibiting bacterial growth remain poorly understood [50]. It can be seen that the bacteria continued to grow in the presence of IO-NPs at the beginning of incubation (1-3 h). At the same time, this growth slows significantly after 3 hours (3-6 hours). The mechanism of reducing the growth of bacteria is still not clear in the literature. Still, potentially, it is suggested that NPs cause oxidative stress after penetrating the bacteria member, then may act as an antioxidant by reacting with any reactive oxygen species (ROS) [51], as well as the dropping of bacterial growth, perhaps because of their large specific surface area and ability to release electrons [52]. In this work, IO-NPs functionalized by chemical ligands showed less effect against the bacteria than IO-NPs functionalized by Teucrium extract. The reason for this possibility is that the surface activity of the IO-NPs synthesized chemically decreases with time, and there is a possibility for oxidation or aggregation of NPs inside the bacteria, which affects its growth [52].

In comparison between the types of chemically synthesized IO-NPs here, it can be seen that the IO-NP capped by DIA ligand has the highest effect on the growth of the bacteria (see Figure 8 (A)). In contrast, the growth of bacteria was slightly increased when IO-NP was capped by AB ligand. The effect of DIA-IO-NPs on the bacteria growth was significant and had a clear bactericide effect through the beginning of the incubation, as shown by the decrease in bacterial growth (see Figure 8 (A) below). It is worth mentioning that the surface chemistry of IO-NPs plays a significant role in the practical implementation of *in vitro* and *in vivo* applications [7]. For example, the antimicrobial effect of IO-NPs depends on the particle size and type of surface coating [38], where differently functionalized IONPs lead to different antibacterial properties, which confirms our results. It is well known that a high surface-to-volume ratio is commonly accompanied by increased production of reactive oxygen species such as free radicals. These characteristics permit IO-NPs to interact closely with bacterial membranes, damaging their structure and leading to the inactivation of bacteria [53].

In addition, Figure 8 shows that the bioactivity of IO-NPs was dependent upon the type of functionalized ligand. For instance, IO-NPs-functionalized by AD ligand showed high biocompatibility and good activity against the bacteria. The reason may be a result of the end-group (free NH_2 group) in this compound. In contrast, IO-NP functionalized by AB showed medium effects. As mentioned in the previous study, the small size of IO-NPs could be the reason for the increasing biological properties of the NPs that penetrate the cell wall of bacteria and produce oxidative stress, damaging the protein and DNA of the bacterial cell [49].

The OD data in Figure 8 (D) show that longer exposure times (> 6 h) are required to achieve a high antibacterial impact of IO-NP functionalized by extracting Teucrium, which demonstrated the highest activity in this study and confirms the previous study [54]. This is because this extract contains phenolic compounds that offer high activity against the bacteria in comparison with chemical ligands that contain amino and carboxyl groups, as shown in Figure 8 (A to D); also, due to its structure, which has a good affinity toward bacterial cells and can easily penetrate the membrane of bacterial cells and inhibit them compared with previous data [55].

These findings revealed the impact of the targeting ligands on the bioactivity of nanoparticles, and that is in line with those of previously published works [27]. When comparing the bio-activity properties of the different IO-NPs functionalized by different

ligands, we found that ligands containing carboxyl, hydroxyl, and amino groups are the best for stabilizing the IO-NPs, which can interact with the surface of IO-NPs by a coordination process [56] and offer biocompatibility at the same time. Furthermore, the NPs' size is considered an important factor controlling their characteristics [57]. For this reason, the smallest size of chemically IO-NPs was produced and showed high effectiveness against bacterial cells in this study. Based on the literature, the binding potential of NPs with small diameters less than 22 nm is expected to be a promising strategy for future development in bio-applications, such as being used for magnetic resonance imaging [57]. Our data show that the IO-NPs synthesized by these chemical ligands had high stability and biocompatibility. Still, the IO-NPs synthesized using green synthesis had the greatest impact on bacteria growth. This impact increased as much as the incubation time increased (nearly 6 h). Thus, the longer incubation time with IO-NP-plant extract caused a more damaging effect on the bacterial cell, which could be successfully used in the future to overcome antibiotic resistance in bacteria.
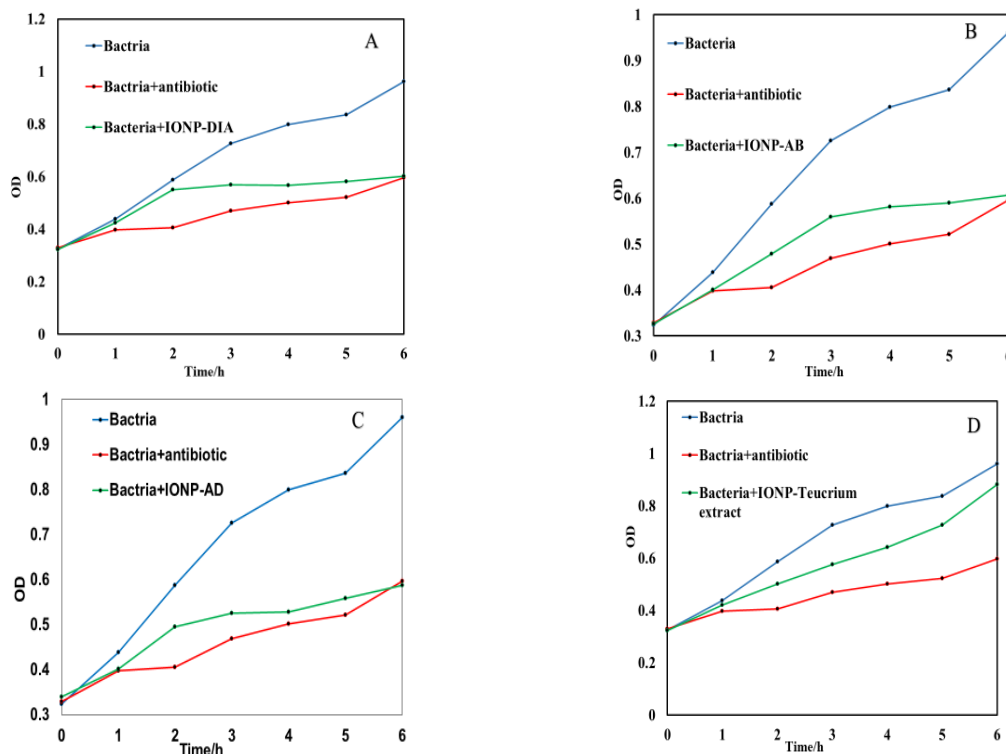

Figure 8. Shows growth curves of *pseudomonas aeruginosa* bacteria treated with (**A** =DIA-IO-NP), (**B**= AB-IO-NP), (**C**=AD-IO-NP), and (**D**= *Teucrium extract*-IO-NP) with antibiotic imipenem10 ug (red curve) at various times in comparison to IO-NP**s** (P < 0.05). The control sample (blue curve) is bacteria without nanoparticles and is used as a reference. Obviously, all the samples show a bactericidal effect, such as a significant decrease in OD with time.

4. Conclusions

In this study, IO-NPs were successfully functionalized using novel ligands for the first time to our knowledge and applied to bioapplications. Moreover, these dispersed-water IO-NPs were free of aggregation and exhibited excellent stability for a long time. The resulting IO-NPs have a biocompatible surface against Pseudomonas aeruginosa bacteria.

The size of IO-NPs ranged from 6 nm to 51 nm based on dynamic light scattering results. The stable IO-NPs were formed at a specific pH (5-7). The effect of the pH on IO-NPs produced was done in acidic and basic conditions (pH 1.4 to pH 13). The IO-NPs are not stable in high or low alkaline or acidic environments, and aggregation was observed when the pH was

increased to 9 and at low pH 2. This confirms that the change in pH of water-dispersed IO-NPs affected their stability.

The comparison between chemical ligands and plant extracts functionalized IO-NPs was done. IO-NPs functionalized by extract plant showed potential antibacterial activity against pseudomonas aeruginosa compared with chemically IO-NP synthesized. Overall, our findings show that the IO-NPs synthesized by these ligands and extract *Teucrium* had good stability and biocompatibility, which encourages researchers to improve them and focus on these IO-NPs for future bioapplication.

Funding

Acknowledgments

Conflicts of Interest

The authors declare no conflict of interest.

References

1. Jiang, K.; Zhang, L.; Bao, G. Magnetic iron oxide nanoparticles for biomedical applications. *Current Opinion in Biomedical Engineering* **2021,** *20*, 100330, https://doi.org/10.1016/j.cobme.2021.100330.

2. Gupta, A.K.; Gupta, M. Synthesis and surface engineering of iron oxide nanoparticles for biomedical applications. *Biomaterials* **2005,** *26*, 3995-4021, https://doi.org/10.1016/j.biomaterials.2004.10.012.

3. Wu, W.; He, Q.; Jiang, C. Magnetic iron oxide nanoparticles: synthesis and surface functionalization strategies. *Nanoscale Research Letters* **2008,** *3*, 397, https://doi.org/10.1007/s11671-008-9174-9.

4. Montiel Schneider, M.G.; Martín, M.J.; Otarola, J.; Vakarelska, E.; Simeonov, V.; Lassalle, V.; Nedyalkova, M. Biomedical Applications of Iron Oxide Nanoparticles: Current Insights Progress and Perspectives. *Pharmaceutics* **2022,** *14*, 204, https://doi.org/10.3390/pharmaceutics14010204.

5. Soetaert, F.; Korangath, P.; Serantes, D.; Fiering, S.; Ivkov, R. Cancer therapy with iron oxide nanoparticles: Agents of thermal and immune therapies. *Advanced Drug Delivery Reviews* **2020,** *163-164*, 65-83, https://doi.org/10.1016/j.addr.2020.06.025.

6. Grauer, O.; Jaber, M.; Hess, K.; Weckesser, M.; Schwindt, W.; Maring, S.; Wölfer, J.; Stummer, W. Combined intracavitary thermotherapy with iron oxide nanoparticles and radiotherapy as local treatment modality in recurrent glioblastoma patients. *Journal of Neuro-Oncology* **2019,** *141*, 83-94, https://doi.org/10.1007/s11060-018-03005-x.

7. Ganapathe, L.S.; Mohamed, M.A.; Mohamad Yunus, R.; Berhanuddin, D.D. Magnetite (Fe$_3$O$_4$) nanoparticles in biomedical application: From synthesis to surface functionalisation. *Magnetochemistry* **2020,** *6*, 68, https://doi.org/10.3390/magnetochemistry6040068.

8. Erdoğan, Ö.; Paşa, S.; Demirbolat, G. M.; Çevik, Ö. Green biosynthesis, characterization, and cytotoxic effect of magnetic iron nanoparticles using Brassica Oleracea var capitata sub var rubra (red cabbage) aqueous peel extract. *Turkish Journal of Chemistry* **2021,** *45*, 1086-1096, https://doi.org/10.3906/kim-2102-2.

9. Sangaiya, P.; Jayaprakash, R. A review on iron oxide nanoparticles and their biomedical applications. *Journal of Superconductivity and Novel Magnetism* **2018,** *31*, 3397-3413, https://doi.org/10.1007/s10948-018-4841-2.

10. Kumar, R.; Pulikanti, G.R.; Shankar, K.R.; Rambabu, D.; Mangili, V.; Kumbam, L.R.; Sagara, P.S.; Nakka, N.; Yogesh, M. Surface coating and functionalization of metal and metal oxide nanoparticles for biomedical

applications. *In*: *Mondal, K (Ed.) Metal Oxides for Biomedical and Biosensor Applications* **2002**, Elsevier, https://doi.org/10.1016/C2019-0-04633-X.

11. Frankamp, B.L.; Boal, A.K.; Tuominen, M.T.; Rotello, V.M. Direct control of the magnetic interaction between iron oxide nanoparticles through dendrimer-mediated self-assembly. *Journal of the American Chemical Society* **2005**, *127*, 9731-9735, https://doi.org/10.1021/ja051351m.

12. Aboyewa, J.A.; Sibuyi, N.R.; Meyer, M.; Oguntibeju, O.O. Green synthesis of metallic nanoparticles using some selected medicinal plants from Southern Africa and their biological applications. *Plants* **2021,** *10*, 1929, https://doi.org/10.3390/plants10091929.

13. Stankovic, M.S.; Curcic, M.G.; Zizic, J.B.; Topuzovic, M.D.; Solujic, S.R.; Markovic, S.D. Teucrium plant species as natural sources of novel anticancer compounds: antiproliferative, proapoptotic and antioxidant properties. *International Journal of Molecular Sciences* **2011,** *12*, 4190-4205, https://doi.org/10.3390/ijms12074190.

14. Coricovac, D.-E.; Moacă, E.-A.; Pinzaru, I.; Cîtu, C.; Soica, C.; Mihali, C.-V.; Păcurariu, C.; Tutelyan, V. A.; Tsatsakis, A.; Dehelean, C.-A. Biocompatible colloidal suspensions based on magnetic iron oxide nanoparticles: synthesis, characterization and toxicological profile. *Frontiers in Pharmacology* **2017,** *8*, 154, https://doi.org/10.3389/fphar.2017.00154.

15. Xu, Y.; Qin, Y.; Palchoudhury, S.; Bao, Y. Water-soluble iron oxide nanoparticles with high stability and selective surface functionality. *Langmuir* **2011,** *27*, 8990-8997, https://doi.org/10.1021/la201652h.

16. Aji, A.; Kunarti, E.S.; Santosa, S.J. Synthesis of gold nanoparticles using p-aminobenzoic acid and p-aminosalicylic acid as reducing agent. *Indonesian Journal of Chemistry* **2019**, *19*, 68-77, https://doi.org/10.22146/ijc.26839.

17. Suppiah, D.D.; Johan, M.R.Influence of solution pH on the formation of iron oxide nanoparticles. *Materials Research Express* **2018,** *6*, 015008, https://doi.org/10.1088/2053-1591/aae428.

18. Meng, X.; Ryu, J.; Kim, B.; Ko, S. Application of iron oxide as a pH-dependent indicator for improving the nutritional quality. *Clinical Nutrition Research* **2016,** *5*, 172-179, https://doi.org/10.7762/cnr.2016.5.3.172.

19. Andrade, Â.L.; Souza, D.M.; Pereira, M.C.; Fabris, J.D.; Domingues, R.Z. pH effect on the synthesis of magnetite nanoparticles by the chemical reduction-precipitation method. *Química Nova* **2010**, *33*, 524-527, https://doi.org/10.1590/S0100-40422010000300006.

20. Abdussalam-Mohammed, W.; Najem, M.Y.; Errayes, A.O.; Shamsi, S.S.; Darwish, M.O.; Mezoughi, A.B. Synthesis of Highly Stabilized AuNPs Using 3,5-Dinitrobenzoic Acid and Sodium Acetate as Capping Agents in an Aqueous Solution and their Bioactivity. *Journal of Nano Research* **2021,** *70*, 67-79, https://doi.org/10.4028/www.scientific.net/JNanoR.70.67.

21. Zaloga, J.; Janko, C.; Agarwal, R.; Nowak, J.; Müller, R.; Boccaccini, A.R.; Lee, G.; Odenbach, S.; Lyer, S.; Alexiou, C. Different storage conditions influence biocompatibility and physicochemical properties of iron oxide nanoparticles. *International Journal of Molecular Sciences* **2015,** *16*, 9368-9384, https://doi.org/10.3390/ijms16059368.

22. Eustis, S.; El-Sayed, M.A. Why gold nanoparticles are more precious than pretty gold: noble metal surface plasmon resonance and its enhancement of the radiative and nonradiative properties of nanocrystals of different shapes. *Chemical Society Reviews* **2006**, *35*, 209-217, https://doi.org/10.1039/B514191E.

23. Heuer-Jungemann, A.; Feliu, N.; Bakaimi, I. *et al*. The role of ligands in the chemical synthesis and applications of inorganic nanoparticles. *Chemical Reviews* **2019**, *119*, 4819-4880, https://doi.org/10.1021/acs.chemrev.8b00733.

24. Gusrizal, G.; Santosa, S.J.; Kunarti, E.S. Rusdiarso, B. Synthesis of silver nanoparticles by reduction of silver ion with m-hydroxybenzoic acid. *Asian Journal of Chemistry* **2017,** *29*, 1417-1422, https://doi.org/10.14233/ajchem.2017.20436.

25. Pakiari, A.; Jamshidi, Z. Nature and strength of M−S Bonds (M= Au, Ag, and Cu) in binary alloy gold clusters. *The Journal of Physical Chemistry A* **2010**, *114*, 9212-9221, https://doi.org/10.1021/jp100423b.

26. Kundu, S.; Nithiyanantham, U. *In situ* formation of curcumin stabilized shape-selective Ag nanostructures in aqueous solution and their pronounced SERS activity. *RSC Advances* **2013,** *3*, 25278-25290, https://doi.org/10.1039/C3RA44471F.

27. Fang, C.; Veiseh, O.; Kievit, F.; Bhattarai, N.; Wang, F.; Stephen, Z.; Li, C.; Lee, D.; Ellenbogen, R.G.; Zhang, M. Functionalization of iron oxide magnetic nanoparticles with targeting ligands: their physicochemical properties and *in vivo* behavior. *Nanomedicine* **2010,** *5*, 1357-1369, https://doi.org/10.2217/nnm.10.55.

28. Kurlyandskaya, G.V.; Litvinova, L.S.; Safronov, A.P. *et al*. Water-Based suspensions of iron oxide nanoparticles with electrostatic or steric stabilization by chitosan: Fabrication, characterization and biocompatibility. *Sensors* **2017,** *17*, 2605, https://doi.org/10.3390/s17112605.

29. Nickels, M.; Xie, J.; Cobb, J.; Gore, J.C.; Pham, W. Functionalization of iron oxide nanoparticles with a versatile epoxy amine linker. *Journal of Materials Chemistry* **2010,** *20*, 4776-4780, https://doi.org/10.1039/C0JM00808G.

30. Lakshminarayanan, S.; Shereen, M.F.; Niraimathi, K.; Brindha, P.; Arumugam, A. One-pot green synthesis of iron oxide nanoparticles from *Bauhinia tomentosa*: Characterization and application towards synthesis of 1,3 diolein. *Scientific Reports* **2021,** *11*, 8643, https://doi.org/10.1038/s41598-021-87960-y.

31. Miri, A.; Najafzadeh, H.; Darroudi, M.; Miri, M.J.; Kouhbanani, M.A.J.; Sarani, M. Iron oxide nanoparticles: biosynthesis, magnetic behavior, cytotoxic effect. *ChemistryOpen* **2021,** *10*, 327-333, https://doi.org/10.1002/open.202000186.

32. Babick, F. Dynamic light scattering (DLS). *In: Hodoroaba, V.D., Unger, W.E.S., Shard, A.G. (Eds) Characterization of Nanoparticles: Measurement Processes for Nanoparticles* **2020**, Elsevier, https://doi.org/10.1016/C2017-0-00312-9.

33. Wittmann, L.; Turrina, C.; Schwaminger, S.P. The Effect of pH and Viscosity on Magnetophoretic Separation of Iron Oxide Nanoparticles. *Magnetochemistry* **2021,** *7*, 80, https://doi.org/10.3390/magnetochemistry7060080.

34. Socoliuc, V.; Peddis, D.; Petrenko, V.I.; Avdeev, M.V.; Susan-Resiga, D.; Szabó, T.; Turcu, R.; Tombácz, E.; Vékás, L. Magnetic nanoparticle systems for nanomedicine—A materials science perspective. *Magnetochemistry* **2020,** *6*, 2, https://doi.org/10.3390/magnetochemistry6010002.

35. Kucuksayan, E.; Bozkurt, F.; Yilmaz, M.T.; Sircan-Kucuksayan, A.; Hanikoglu, A.; Ozben, T. A new combination strategy to enhance apoptosis in cancer cells by using nanoparticles as biocompatible drug delivery carriers. *Scientific Reports* **2021,** *11*, 13027, https://doi.org/10.1038/s41598-021-92447-x.

36. Tomaszewska, E.; Soliwoda, K.; Kadziola, K.; Tkacz-Szczesna, B.; Celichowski, G.; Cichomski, M.; Szmaja, W.; Grobelny, J. Detection limits of DLS and UV-VIS spectroscopy in characterization of polydisperse nanoparticles colloids. *Journal of Nanomaterials* **2013,** *2013*, 313081, https://doi.org/10.1155/2013/313081.

37. Wang, L.; Housel, L.M.; Bock, D.C.; Abraham, A.; Dunkin, M.R.; McCarthy, A.H.; Wu, Q.; Kiss, A.; Thieme, J.; Takeuchi, E.S. Deliberate Modification of Fe_3O_4 Anode Surface Chemistry: Impact on Electrochemistry. *ACS Applied Materials Interfaces* **2019,** *11*, 19920-19932, https://doi.org/10.1021/acsami.8b21273.

38. Saladino, G.M.; Hamawandi, B.; Demir, M.A.; Yazgan, I.; Toprak, M.S. A versatile strategy to synthesize sugar ligand coated superparamagnetic iron oxide nanoparticles and investigation of their antibacterial activity. *Colloids and Surfaces A: Physicochemical and Engineering Aspects* **2021,** *613*, 126086, https://doi.org/10.1016/j.colsurfa.2020.126086.

39. Do, B.P.H.; Nguyen, B.D.; Nguyen, H.D.; Nguyen, P.T. Synthesis of magnetic composite nanoparticles enveloped in copolymers specified for scale inhibition application. *Advances in Natural Sciences: Nanoscience and Nanotechnology* **2013,** *4*, 045016, https://doi.org/10.1088/2043-6262/4/4/045016.

40. Alvarez-Ros, M.; Sánchez-Cortés, S.; Garcıa-Ramos, J. Vibrational study of the salicylate interaction with metallic ions and surfaces. *Spectrochimica Acta Part A: Molecular and Biomolecular Spectroscopy* **2000,** *56*, 2471-2477, https://doi.org/10.1016/S1386-1425(00)00328-0.

41. Song, X.; Sun, S.; Zhang, W.; Yin, Z. A method for the synthesis of spherical copper nanoparticles in the organic phase. *Journal of Colloid and Interface Science* **2004,** *273*, 463-469, https://doi.org/10.1016/j.jcis.2004.01.019.

42. Fadwa, A.O.; Alkoblan, D.K.; Mateen, A.; Albarag, A.M. Synergistic effects of zinc oxide nanoparticles and various antibiotics combination against *Pseudomonas aeruginosa* clinically isolated bacterial strains. *Saudi Journal of Biological Sciences* **2021,** *28*, 928-935, https://doi.org/10.1016/j.sjbs.2020.09.064.

43. Borcherding, J.; Baltrusaitis, J.; Chen, H.; Stebounova, L.; Wu, C.-M.; Rubasinghege, G.; Mudunkotuwa, I.A.; Caraballo, J.C.; Zabner, J.; Grassian, V.H.; Comellas, A.P. Iron oxide nanoparticles induce Pseudomonas aeruginosa growth, induce biofilm formation, and inhibit antimicrobial peptide function. *Environmental Science: Nano* **2014,** *1*, 123-132, https://doi.org/10.1039/C3EN00029J.

44. Seabra, A.B.; Pelegrino, M.T.; Haddad, P.S. Antimicrobial applications of superparamagnetic iron oxide nanoparticles: Perspectives and challenges. *In: Ficai, A., Grumezescu, A. (Eds) Nanostructures for Antimicrobial Therapy* **2017,** Elsevier, https://doi.org/10.1016/B978-0-323-46152-8.00024-X.

45. Ali, A.; Hira Zafar, M.Z.; Ul Haq, I.; Phull, A.R.; Ali, J.S.; Hussain, A. Synthesis, characterization, applications, and challenges of iron oxide nanoparticles. *Nanotechnology, Science and Applications* **2016,** *9*, 49-67, https:// doi.org/10.2147/NSA.S99986.

46. Zhao, S.; Yu, X.; Qian, Y.; Chen, W.; Shen, J. Multifunctional magnetic iron oxide nanoparticles: an advanced platform for cancer theranostics. *Theranostics* **2020,** *10*, 6278-6309, https://doi.org/10.7150/thno.42564.

47. Thakur, M.; Poojary, S.; Swain, N. Green Synthesis of Iron Oxide Nanoparticles and Its Biomedical Applications. *In: Saglam, N., Korkusuz, F., Prasad, S. (Eds.) Nanotechnology Applications in Health and Environmental Sciences. Nanotechnology in the Life Sciences* **2021**, Springer, Cham, https://doi.org/10.1007/978-3-030-64410-9_5.

48. Gudkov, S.V.; Burmistrov, D.E.; Serov, D.A.; Rebezov, M.B.; Semenova, A.A.; Lisitsyn, A.B. Do iron oxide nanoparticles have significant antibacterial properties? *Antibiotics* **2021,** *10*, 884, https://doi.org/10.3390/antibiotics10070884.

49. Vasantharaj, S.; Sathiyavimal, S.; Senthilkumar, P.; LewisOscar, F.; Pugazhendhi, A. Biosynthesis of iron oxide nanoparticles using leaf extract of *Ruellia tuberosa*: antimicrobial properties and their applications in photocatalytic degradation. *Journal of Photochemistry and Photobiology B: Biology* **2019,** *192*, 74-82, https://doi.org/10.1016/j.jphotobiol.2018.12.025.

50. Simon-Deckers, A.; Loo, S.; Mayne-L'hermite, M.; Herlin-Boime, N.; Menguy, N.; Reynaud, C.; Gouget, B.; Carriere, M. Size-, composition-and shape-dependent toxicological impact of metal oxide nanoparticles and carbon nanotubes toward bacteria. *Environmental Science & Technology* **2009,** *43*, 8423-8429, https://doi.org/10.1021/es9016975.

51. Ševců, A.; El-Temsah, Y.S.; Joner, E.J.; Černík, M. Oxidative stress induced in microorganisms by zero-valent iron nanoparticles. *Microbes and Environments* **2009**, *26*, 271-281, https://doi.org/10.1264/jsme2.ME11126.

52. Liu, J.; Vipulanandan, C.; Cooper, T.F.; Vipulanandan, G. Effects of Fe nanoparticles on bacterial growth and biosurfactant production. *Journal of Nanoparticle Research* **2013,** *15*, 1405, https://doi.org/10.1007/s11051-012-1405-4.

53. Thukkaram, M.; Sitaram, S.; Kannaiyan, S.K.; Subbiahdoss, G. Antibacterial efficacy of iron-oxide nanoparticles against biofilms on different biomaterial surfaces. *International Journal of Biomaterials* **2014,** *2014*, 716080, https://doi.org/10.1155/2014/716080.

54. Velsankar, K.; Parvathy, G.; Mohandoss, S.; Krishna Kumar, M.; Sudhahar, S. *Celosia argentea* leaf extract-mediated green synthesized iron oxide nanoparticles for bio-applications. *Journal of Nanostructure in Chemistry* **2022**, *12*, 625-640, https://doi.org/10.1007/s40097-021-00434-5.

55. Bilal, M.; Iqbal, H.M.; Adil, S.F.; Shaik, M.R.; Abdelgawad, A.; Hatshan, M.R.; Khan, M. Surface-coated magnetic nanostructured materials for robust bio-catalysis and biomedical applications-A review. *Journal of Advanced Research* **2022**, *38*, 157-177, https://doi.org/10.1016/j.jare.2021.09.013.

56. Begin-Colin, S.; Felder-Flesch, D. Functionalisation of magnetic iron oxide nanoparticles. *In: Thanh, N (Ed.) Magnetic nanoparticles: from fabrication to clinical applications* **2012**, CRC Press, Boca Raton, https://doi.org/10.1201/b11760.

57. Hofmann, A.; Thierbach, S.; Semisch, A.; Hartwig, A.; Taupitz, M.; Rühl, E.; Graf, C. Highly monodisperse water-dispersable iron oxide nanoparticles for biomedical applications. *Journal of Materials Chemistry* **2010,** *20*, 7842-7853, https://doi.org/10.1039/C0JM01169J.